Clinical Proteomics

RESEARCH

Open Access

Quantitative enrichment of amyloid precursors refines mass spectrometry-based amyloidosis diagnosis

Sylvaine Di Tommaso[1,2†], Bertrand Chauveau[3,4†], Cyril Dourthe[1,2], Jean-William Dupuy[2,5], Frédéric Saltel[1,2*], Brigitte Le Bail[1,3†] and Anne-Aurélie Raymond[1,2†]

Abstract

Introduction Amyloidosis typing is crucial to determine the best therapeutic strategy for patients. Since conventional histological techniques often fail, the identification of amyloid precursors by mass spectrometry has become the new standard. However, without quantification, selecting the amyloid precursor from proteins that may be ubiquitous under non-pathological conditions can be equivocal. Therefore, we quantified protein enrichment in amyloid deposits to improve amyloidosis typing.

Methods Protein enrichment was measured by extracted ion chromatogram-based label-free quantification by comparing a microdissected amyloid area to a non-amyloid area. We assessed the discrimination ability of candidate precursors with this approach compared to the two practiced identification methods.

Results As a proof of concept, we selected 9 cases including the most common amyloidosis subtypes, 6 typed by immunohistochemistry and 3 inconclusive by immunohistochemistry. Proteins associated with amyloid deposits were identified in all samples, confirming the pathology. Where the routine clinical mass spectrometric identification techniques allowed unambiguous conclusions for 3 of 9 cases, quantification of the enrichment ratio in amyloid deposits allowed unambiguous precursor selection in all cases.

Conclusion Quantification of precursor enrichment in amyloid deposits is a promising optimization for amyloidosis typing, which should be studied in larger cohorts. Incorporated into routine clinical processes, it could improve patient care in difficult diagnostic situations.

Keywords Amyloidosis typing, Label-free quantification, Mass spectrometry, Proteomics

†Sylvaine Di Tommaso, and Bertrand Chauveau contributed equally, Brigitte Le Bail and Anne-Aurélie Raymondjointly supervised this work .

*Correspondence:
Frédéric Saltel
frederic.saltel@inserm.fr

Full list of author information is available at the end of the article

Graphical Abstract

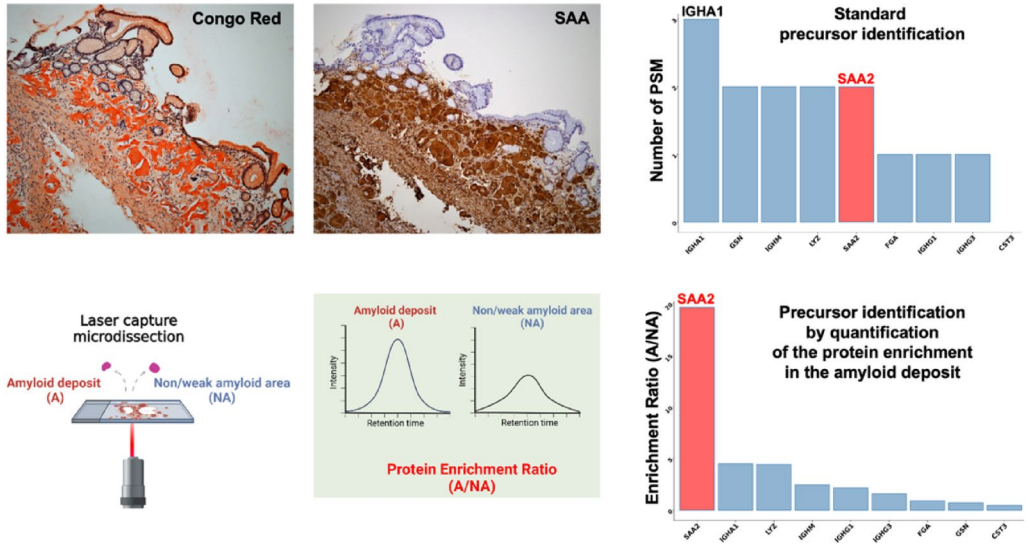

Introduction

Amyloidoses are rare, heterogeneous diseases caused by the extracellular deposition of amyloid, a fibrillar material composed of twisted β-sheet protein aggregates [1, 2]. Depending on the site of deposition and the mechanism of protein misfolding, amyloidosis can be systemic or localized, acquired or hereditary. Amyloid deposits contain a disease-specific precursor protein along with common components such as heparan sulfate proteoglycan and serum amyloid P component [2]. The International Amyloidosis Society maintains the list of amyloid precursors, which forms the basis for the nomenclature of amyloidoses. This list continues to expand, with 36 precursors identified in 2018 [3] and 42 to date [4]. The main systemic precursors—immunoglobulin light chains (κ or λ, AL amyloidosis), transthyretin (ATTR, acquired or hereditary), and serum amyloid A (AA)—account for nearly 90% of cases diagnosed in routine practice [5]. Treatment strategies depend on the nature of the precursor and the distribution of deposits, ranging from chemotherapy, immunotherapy, or autologous stem cell transplantation for AL amyloidosis, to inflammation control for AA amyloidosis, and siRNA therapy or liver transplantation in selected hereditary ATTR cases [6]. Accurate amyloid typing is therefore essential for optimal patient management and genetic counseling.

Diagnosis may be clinically suspected or incidentally discovered by pathologists. Still, with few exceptions, confirmation requires histopathological evaluation of an affected tissue or organ. Minor salivary glands, abdominal fat, and colonic mucosa are common biopsy sites, as they are frequently involved and easily accessible. Amyloid deposits show characteristic Congo red positivity and yellow-green birefringence under polarized light. Amyloid typing can be performed by immunofluorescence on frozen tissues or by chromogenic immunohistochemistry (IHC) on formalin-fixed paraffin-embedded (FFPE) samples. However, IHC often suffers from background noise—particularly for light chains [7] and transthyretin [8] — and from the limited availability of antibodies for rare amyloid subtypes. Tissue scarcity can further restrict the number of proteins tested. Immunoelectron microscopy offers an alternative but is available only in few expert centers and requires a dedicated sample.

Over the past decade, mass spectrometry (MS)-based proteomics from FFPE samples has emerged as the gold standard for amyloid typing, representing the first clinical application of MS-based proteomics in diagnostic pathology [5, 9]. It is particularly valuable when conventional methods are inconclusive, contradictory to clinical findings, or non-informative [10]. The Mayo Clinic and the UK National Amyloidosis Centre are the leading reference centers, each reporting hundreds to thousands of accurately typed cases [5, 9, 11]. Rezk et al. demonstrated that MS successfully resolved 80% of previously uninformative cases by IHC [12], while the Mayo Clinic reported a 100% precursor identification rate [5, 9].

Both centers use a similar bottom-up proteomics workflow involving laser microdissection of Congo red-stained deposits, tryptic digestion, and peptide analysis by LC-MS/MS. Amyloid identity is confirmed by detection of shared amyloid-associated proteins, including serum amyloid P component, apolipoprotein E, and apolipoprotein A-IV [5, 11]. For precursor identification, the Mayo Clinic selects the protein with the highest number

of peptide spectrum matches (PSMs), whereas the UK Centre uses the protein with the best Mascot identification score [11, 13, 14]. Despite these robust pipelines, precursor assignment can remain challenging when multiple candidates show comparable PSM or Mascot scores, as observed in samples with scarce deposits, blood contamination, or proteins naturally present in tissues such as apolipoproteins A-I/A-IV, immunoglobulins, or transthyretin [11, 12, 15]. An Australian group reported up to 40% of AL amyloidosis cases displaying secondary precursors with similar PSM values [16].

Protein identification by MS depends on intrinsic physicochemical properties, such as peptide ionization efficiency and sequence length. Consequently, low-abundance proteins with well-ionizing peptides may yield stronger signals than abundant proteins with poor ionization. Conventional proteomic analysis therefore restricts quantification to comparisons of identical peptides (same sequence, charge, and modifications) and does not consider inter-protein comparisons of identification scores, PSMs, or relative intensities as valid measures of abundance [17].

To enhance diagnostic confidence, targeted quantitative MS approaches have been proposed. These rely on isotopically labeled standard peptides to quantify specific amyloid precursors. Ogawa et al. provided the first proof of concept [18], and Park et al. demonstrated high sensitivity and specificity of targeted quantification compared with standard MS-based identification, though only for the three major systemic forms—AL, AA, and ATTR [19]. These pseudo-absolute quantification methods require advanced MS expertise and specialized acquisition workflows, limiting their use in clinical laboratories. Extracted Ion Chromatogram-based (XIC-based) label-free quantification (LFQ) is widely used in exploratory proteomics and increasingly applied to clinical studies [20, 21]. XIC-based LFQ estimates protein abundance by extracting ion chromatograms (XICs) based on retention time and m/z coordinates, enabling relative quantification even when peptides are not consistently identified, provided they are sequenced at least once. This approach allows direct comparison of relative protein abundances between samples, making it particularly suitable for evaluating the enrichment of precursor proteins within amyloid deposits.

To our knowledge, no study has assessed XIC-based amyloid precursor enrichment quantification using a label-free approach in FFPE-derived samples as compared to conventional reported approaches. In this study, we propose to implement XIC-based label-free enrichment quantification in routine practice to improve the robustness and reliability of amyloidosis typing.

Materials and methods

Study population

This study relied on a retrospective inclusion of selected patients with an amyloidosis diagnosis performed at the Bordeaux University Hospital from 2013 to 2022, with consistent clinico-biological data. Archived formalin-fixed and paraffin embedded (FFPE) samples with sufficient remaining material were included. Moreover, the selection process, for a small yet diverse cohort, relied on the specimen type (biopsy or surgical specimen, tissue), the ground truth amyloid type, the localized or systemic nature of the deposits and the informative nature of IHC. Main clinical, biological and pathological characteristics were retrieved from the institutional medical software. Congo red staining was performed for amyloidosis diagnosis in all samples and amyloidosis typing was performed by routine immunohistochemistry targeting kappa and lambda light chains (clone A21-Y and K22-Y from Clinisciences), serum amyloid A (clone MC 1 from Dako), transthyretin (polyclonal from Dako) and β2-microglobulin (polyclonal from Genetex). All immunostains were performed using an Omnis automate from Dako Agilent (EnVision Flex/horseradish peroxidase for signal amplification). All reagents were provided by Dako/Agilent. No frozen tissue was available for any case. For each case, the abundance of amyloid deposits was semi-quantitatively assessed by a pathologist in a 1 to 5 scale, where 5 represents a sample nearly exclusively affected by amyloid deposits.

The study was conducted according to the guidelines of the Declaration of Helsinki and was approved by a local ethic committee for the protection of persons (reference number CER-BDX-2023-02).

Microdissection of selected area and sample preparation

For each sample, 5 µm thick sections were cut from FFPE blocks on polyethylene naphthalate covered slides. Paraffin removal, rehydration and color staining were performed using the following baths: xylene (5 min), xylene (overnight), 2 ethanol absolute baths (1 min), ethanol 95 (1 min), water (1 min), Hematoxylin (1 min), water (until clear bath). Non-amyloid (NA) and Amyloid (A) areas were selected from the Hematoxylin eosin saffron or Congo red slides performed for diagnosis purposes, under the supervision of a pathologist (either B.LB. or B.C.). Areas between 0.1 and 1 mm^2 were microdissected with a PALM type 4 (Zeiss) laser microdissector (same size for each NA/A pair). Sections were collected, immersed in a 50 mM Ammonium bicarbonate buffer, and heated at 90 °C for 120 min with occasional vortexing. Samples were reduced in 30 mM dithiothreitol at 56 °C, alkylated in 900 mM iodoacetamide in dark and digested overnight with 10 µL of 0.01 µg/µL of trypsin.

Peptides were then analyzed by liquid chromatography and tandem mass spectrometry (LC-MS/MS).

Mass spectrometry analysis

NanoLC-MS/MS analysis was performed using an Ultimate 3000 RSLC Nano-UPHLC system (Thermo Scientific, USA) coupled to a nanospray Orbitrap Fusion™ Lumos™ Tribrid™ Mass Spectrometer (Thermo Fisher Scientific, California, USA). Each peptide extracts were loaded on a 300 µm ID x 5 mm PepMap C_{18} precolumn (Thermo Scientific, USA) at a flow rate of 10 µL/min. After a 3 min desalting step, peptides were separated on a 50 cm EasySpray column (75 µm ID, 2 µm C_{18} beads, 100 Å pore size, ES903, Thermo Fisher Scientific) with a 4–40% linear gradient of solvent B (0.1% formic acid in 80% ACN) in 57 min. The separation flow rate was set at 300 nL/min. The mass spectrometer operated in positive ion mode at a 2.0 kV needle voltage. Data was acquired using Xcalibur 4.4 software in a data-dependent mode. MS scans (m/z 375–1500) were recorded at a resolution of R = 120,000 (@ m/z 200), a standard AGC target and an injection time in automatic mode, followed by a top speed duty cycle of up to 3 s for MS/MS acquisition. Precursor ions (2 to 7 charge states) were isolated in the quadrupole with a mass window of 1.6 Th and fragmented with HCD@28% normalized collision energy. MS/MS data was acquired in the Orbitrap cell with a resolution of R = 30,000 (@m/z 200), a standard AGC target and a maximum injection time in automatic mode. Selected precursors were excluded for 60 s. For protein identification, Mascot 2.5 algorithm through Proteome Discoverer 2.5 Software (Thermo Fisher Scientific Inc.) was used in batch mode by searching against the UniProt Homo sapiens database (79 071 entries, Reference Proteome Set, release date: January, 2022) from http://www.uniprot.org/ website. Two missed enzyme cleavages were allowed for trypsin. Mass tolerances in MS and MS/MS were set to 10 ppm and 0.02 Da. Oxidation of methionine and acetylation of lysine were searched as dynamic modifications. Carbamidomethylation on cysteine was searched as static modification. Raw LC-MS/MS data were imported in Proline Studio for feature detection, alignment, and quantification [22]. Briefly, all detected LC-MS peaks were associated with validated PSMs (iterative alignment). The parameters for m/z alignment tolerance and retention time alignment tolerance are 10.0 ppm and 300 s, respectively. Match between runs were set with m/z tolerance of 10 ppm and a time tolerance of 60 seconds to overlay all the two-dimensional (m/z and retention time) feature maps. The abundance of each ion is estimated from the apex of the chromatographic peak. Map intensities were normalized using median ratio method. Proteins identification was accepted only with at least 2 specific peptides with a pretty rank = 1 and with a protein False Discovery Rate (FDR) value less than 1.0% calculated using the "decoy" option in Mascot. Label-free quantification of MS1 spectra by extracted ion chromatograms (XIC) was carried out with parameters indicated previously [23]. The mass spectrometry proteomics data have been deposited to the ProteomeXchange Consortium via the PRIDE [24] partner repository with the dataset identifier PXD039814.

Bioinformatical and statistical analysis

Statistical analyses and plots were performed using R, version 4.2.2 [25]. Plots were performed using the ggplot2 package and the ggpubr package. Spearman's rank correlations were performed using the stats package. To assess the confidence in data interpretation, we defined a confidence score for each approach, expressed as a ratio (score of the first precursor divided by the mean of the next 2 scores). As all three methods of mass spectrometry-based amyloidosis typing hypothesized that, from all identified and/or quantified proteins, a protein precursor with a top score will emerge (PSM, Mascot or abundance ratio), confidence in results interpretation can be summarized, for each approach, as the relative difference between the protein precursor with the best score compared to the next two scores.

Results

Clinical and biological characteristics of the patients

We selected a panel of 9 cases as a proofofconcept, focusing on the most common amyloidosis types. For 6 of them, immunohistochemistry (IHC) was informative. For 3 of them, IHC was not informative but the associated clinical data of the patient strongly suggested the amyloid precursor determination. Of these 9 patients, 8 were cases of systemic amyloidosis (case numbers 1 to 6, 8 and 9) and 1 was a case of localized amyloidosis (case 7). Mean age of included patients was 68 years old (range 47–83). Available samples consisted of a biopsy for 6 cases and a surgical specimen for 3 cases, from various organ or tissue origin (Table 1). Amyloidosis typing based on clinicopathological findings were as follows: 2 AL lambda, 2 AL kappa, 1 ATTR, 1 Aβ2M and 1 AA. In three cases (cases 4,7 and 8), IHC was non-informative. Case 4 had an IgM kappa monoclonal gammopathy with an incidental finding of amyloid deposits in a duodenal ampulloma resection. Case 7 had a previous biopsy that favored kappa light chain deposits by IHC. Case 8 had a lambda light chain multiple myeloma. Main clinicopathological characteristics are summarized in Table 1.

Table 1 Relevant clinical data of the included patients

Case No.	Age (years)	Gender	Sample (surgical specimen, biopsy)	Site	Amyloid subtype by IHC	Associated condition
1	66	F	Surgical specimen (gangrene)	Perineum	β2-microglobulin	End-stage renal disease with dialysis for 40 years
2	78	M	Biopsy	Minor salivary gland	Light chain Lambda	Multiple myeloma (IgG Lambda)
3	47	F	Biopsy	Rectum	Serum amyloid A-1 protein	Familial Mediterranean fever. Hemodialysis
4	83	M	Surgical specimen	Duodenum (ampulloma)	Non-informative	IgM monoclonal gammopathy (kappa). Suspicion of low-grade digestive lymphoma.
5	56	M	Surgical specimen	Liver (recipient)	Transthyretin	Transthyretin-related hereditary amyloidosis
6	69	F	Biopsy	Bone marrow	Light chain lambda	Monoclonal gammopathy (IgG lambda)
7	70	F	Biopsy	Larynx	Undefined from this sample. A prior biopsy favored kappa light chain deposits.	Localized amyloidosis
8	83	M	Biopsy	Minor salivary gland	Doubtful (moderate staining with transthyretin).	Light chain multiple myeloma (lambda)
9	62	F	Biopsy	Liver	Light chain Kappa	IgM monoclonal gammopathy (kappa).

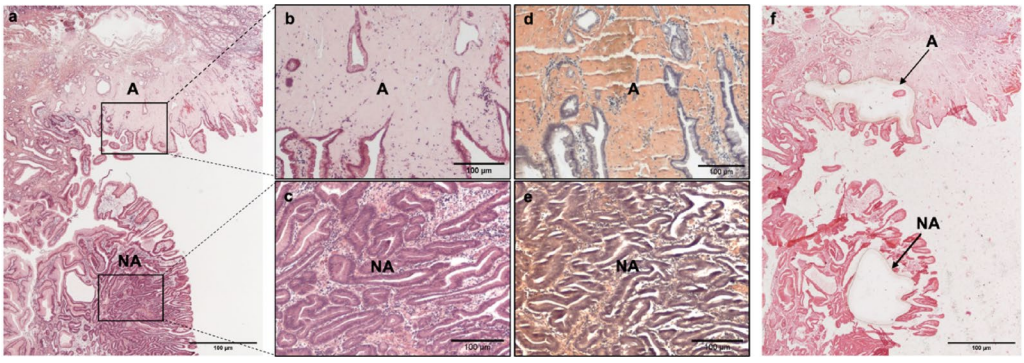

Fig. 1 Laser capture of amyloid (A) and non-amyloid (NA) tissue areas in case number 4. (**a**): Hematoxylin-Eosin-Saffron (HES) staining from a surgical resection of ampulloma. Focus on amyloid deposits seen in the lamina propria and on a non-amyloid area (**b** and **c**, HES staining), and with Congo red staining (**d** and **e**). (**f**): HES section after laser capture. The arrows indicate the microdissected areas. Scale bar = 100 µm

Quantification of protein enrichment in amyloid deposits and comparison with routine identification selection methods

For each case, two regions of interest of the same surface (1 mm^2) were isolated by laser microdissection (Fig. 4), one with amyloid deposits (Fig. 4b) and the other without morphological amyloid deposits (Fig. 4c). These regions were previously annotated on a Congo red staining by an experienced pathologist (Fig. 4d and e). After microdissection (Fig. 4f), proteins were extracted and digested, and proteolytic peptides were analyzed by high resolution tandem mass spectrometry (LC-MS/MS) (Fig. 2a). In the amyloid area, identification of at least two of the three proteins associated with amyloid deposition (serum amyloid P-component/APCS, apolipoprotein E/APOE, and apolipoprotein A-IV/APOA4) was used as an initial quality control. For amyloidosis typing, the two methods routinely used in the expert centers are (i) the PSM, the protein precursor with the most peptide spectra matches (PSM, number of MS/MS spectra) in the amyloid area (A) and (ii) the Mascot score, the precursor with the highest Mascot identification score in the amyloid zone (A). We compared these methods to (iii) the quantification of the enrichment ratio by a label-free approach: the precursor with the highest enrichment ratio calculated by comparing its relative abundance between the amyloid area (A) and the non-amyloid area (NA) (Fig. 2b, Supplementary Table 1). A selection is first made from the known amyloid precursors (systemic and/or localized when applicable), which means that among the identified proteins we do not consider proteins that have never been associated with amyloidosis in first intention. Overall, in all analyzed cases, we identified between 4 and 34 amyloid protein precursors per case. The quantification of the protein enrichment in the deposits (ratio A/NA) revealed that several precursors could be enriched and allowed us to isolate the precursor with the highest enrichment rate. Some ubiquitous amyloid precursors were even more present in the non-amyloid tissue than in the deposits (ratio $A/NA \leq 0.5$). These results demonstrate the interest of providing quantity information beyond the simple identification of precursors (Fig. 2b, Supplementary Table 1). We then focused on each of the analyzed cases. As a first example, case 3 is an inflammatory

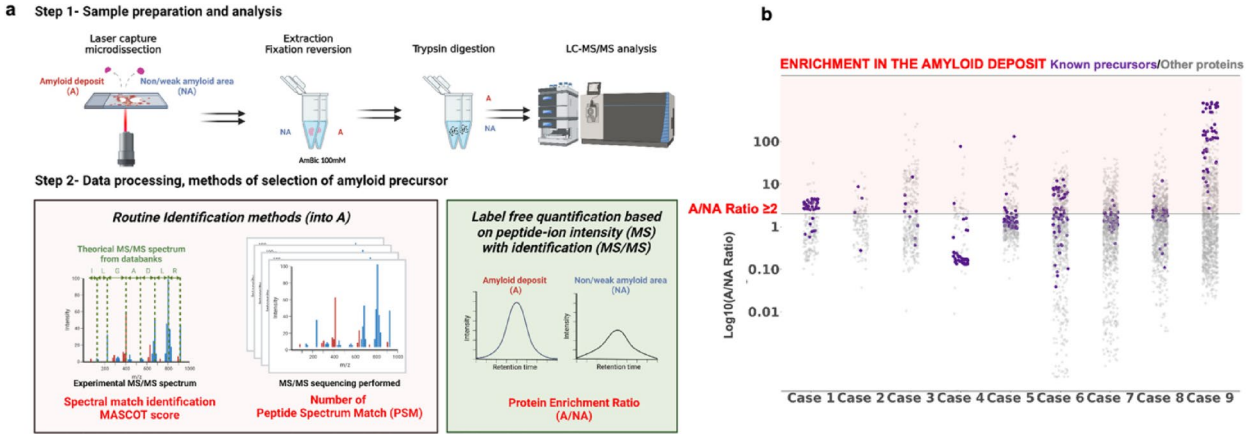

Fig. 2 **a**- Analytical workflow. Step 1 - Microdissection of an amyloid (A) and a non-amyloid (NA) area. Proteins were extracted, digested with trypsin and peptides analyzed by high resolution tandem mass spectrometry (LC-MS/MS). Step 2 - Processing of mass spectrometry (MS) data, the two methods currently practiced in clinical routine are based on the quality of identification from an amyloid area (Mascot score and Peptide Spectrum Match/PSM number). The proposed new method (in green) integrates a quantification of the relative abundances of proteins to quantify an enrichment ratio in the amyloid deposits compared to a non-amyloid area (A/NA). **b**- Global representation of the identified and quantified proteins for the 9 analyzed cases. Each point represents a protein distributed according to its A/NA ratio. Proteins above the bar have an A/NA ratio greater than or equal to 2 and are considered to be enriched in the amyloid deposits (threshold empirically defined). Proteins colored in purple are known precursors of amyloidosis. It should be noted that, in case of an AL amyloidosis, several immunoglobulin fragments can be detected as precursor with the same clinical meaning (e.g., a constant fragment of a kappa light chain and one or several fragments of a kappa variable region, all pointing towards an AL kappa amyloidosis)

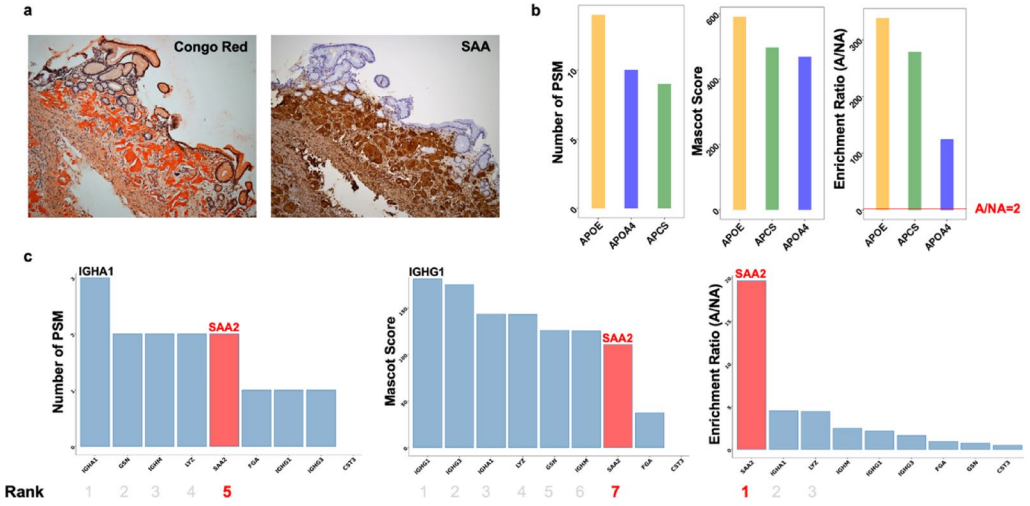

Fig. 3 Graphical representation of the results of case 3. **a**- Congo Red staining and Serum amyloid A (SAA) immunostaining that allowed amyloidosis diagnosis and typing in clinical practice. **b-** Identification and quantification of the enrichment of amyloid-associated proteins. At least two of the three must be found enriched to confirm the presence of amyloid deposits in the sample. Enriched proteins have a relative abundance ratio (amyloid area (A) to non-amyloid area (NA)) far greater than 2 (red bar). **c-** Ranking results according to the 2 clinical routine identification methods (Mascot score and number of PSM) and ranking of enrichment ratios in the amyloid deposits. The protein associated with the known amyloidosis type is colored in red and its ranking is indicated below. The enrichment ratio is of nearly 20 for serum amyloid A, while other described amyloid precursors only showed a comparatively mild enrichment

AA amyloidosis that was previously characterized by IHC (Fig. 3a). Amyloidosis-associated proteins (APOE, APOA4 and APCS) were identified and were enriched in the deposits (Fig. 3b). The number of PSM and the Mascot score of the SAA2 precursor were ranked fifth and seventh, respectively, among the identified precursors. In contrast, with our quantification method, the highest A/NA enrichment among the amyloid precursors was SAA2 ratio (A/NA = 19.6) (Fig. 3c). Another example is case 8. Here, unlike the previous illustrated case, IHC was not informative for amyloidosis typing, with at best a doubtful and moderate staining with transthyretin, while the patient had a lambda light chain multiple myeloma (Fig. 4a). The quantification ratio confirmed transthyretin as the leading enriched amyloid precursor (ratio A/NA 13.7), while both PSM and Mascot scores

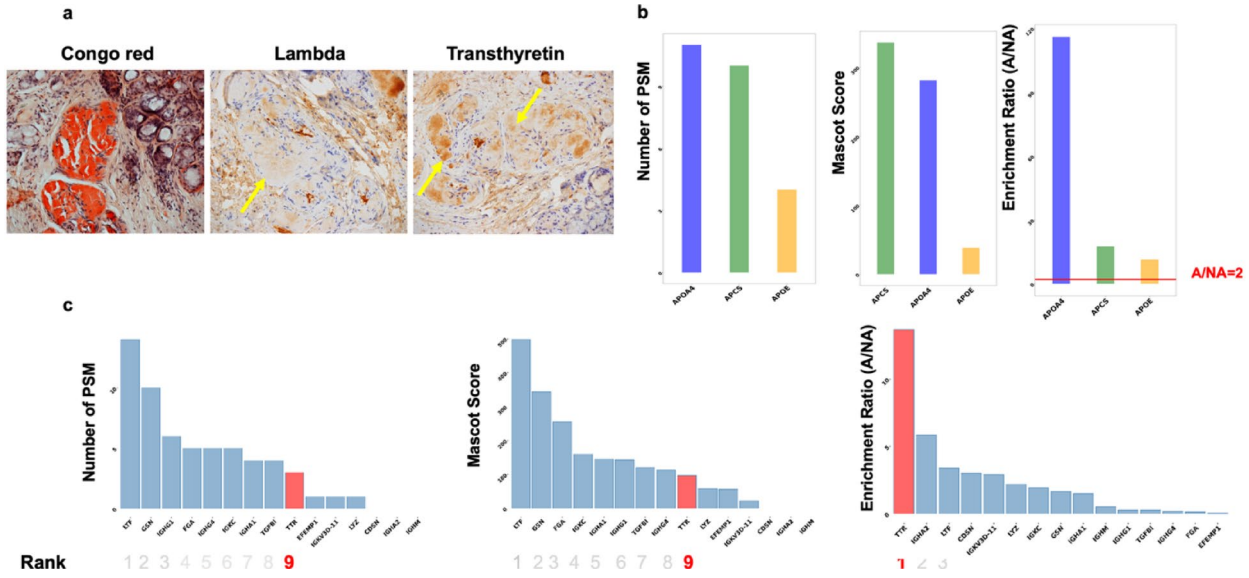

Fig. 4 Graphical representation of the results of the analysis of case 8. **a**- Congo Red staining, showing amyloid deposits in a minor salivary gland sample, with corresponding lambda and transthyretin immunostains. No significant staining is seen with lambda while transthyretin shows at best a moderate staining. **b**- Identification and quantification of the enrichment of amyloid-associated proteins. At least two of the three must be found enriched to confirm the presence of amyloid deposits in the sample. Enriched proteins have a relative abundance ratio (amyloid area (A) to non-amyloid area (NA)) far greater than 2 (red bar). **c**- Ranking results according to the 2 clinical routine identification methods (Mascot score and number of PSM) and ranking of enrichment ratios in the amyloid deposits. The protein associated with the amyloidosis type is colored in red and the first ranking is indicated below. The enrichment ratio is of nearly 14 for transthyretin, while other amyloid precursors only showed a comparatively mild or no enrichment

highlighted Gelsolin as the leading protein precursor of systemic amyloidosis, inconsistent with the clinical data. Of note, lambda light chain was not detected by mass spectrometry in this case, consistent with the IHC findings. These two examples illustrate the gain in robustness in quantifying protein enrichment in amyloid deposition compared to a simple identification approach. Considering case 9, a liver biopsy nearly entirely replaced by kappa light chain amyloid deposits, a microdissection of a non-amyloid area was not possible. Here, we used a pool of subnormal liver tissues as control, coming from surgical specimens of 3 patients, which led to the correct precursor determination of kappa light chain as the leading enriched protein by quantification ratio.

Overall, identification and quantification results of the 9 cases analyzed are summarized in Table 2. Proteins known to be associated with amyloidosis were systematically identified, with varying levels of enrichment in each case. We found a significant and positive correlation between the semi-quantitative histological abundance of amyloid deposits and the APOE PSM score ($\rho = 0.82$, $p = 0.01$) and with the APOE Mascot score ($\rho = 0.86$, $p = 0.006$). No significant correlations were observed with other amyloidosis-associated proteins (number of PSMs or Mascot score), probably due to a lack of statistical power: APCS ($\rho = 0.28$, $p = 0.46$ and $\rho = 0.35$, $p = 0.35$, respectively) and APOA4 ($\rho = 0.29$, $p = 0.49$ and $\rho = 0.29$, $p = 0.49$, respectively). As for the abundance ratio, no correlations were found between the histological amount of amyloid deposits and APOA4 ($\rho = -0.25$, $p = 0.55$), APCS ($\rho = 0.009$, $p = 0.98$) or APOE ($\rho = 0.46$, $p = 0.26$). Considering amyloidosis typing, the PSM number-based and Mascot methods retained a correct amyloid precursor in 3 cases out of 9, while results were equivocal in 5 and misleading in 1. Enrichment quantification retained a correct amyloid precursor in all cases (Table 2.).

At this stage, we wanted to define an indicator allowing us to compare the different approaches based on mass spectrometry. Whatever the approach used, from all identified and/or quantified proteins, a protein precursor with a top score is deemed to emerge (number of PSM, Mascot score or enrichment ratio). Confidence in results interpretation can thus be summarized, for each approach, as the relative difference between the hit protein compared to the other proteins. We defined a confidence score for each approach calculated by dividing the value associated with the hit protein by the average value of the next 2 proteins. In this way, label-free quantification of enrichment in this cohort showed the most confident results compared to PSM- and Mascot-based approaches (Mann-Whitney U tests, $p = 0.002$ and $p = 0.0005$ respectively, Supplementary Fig. 1). No significant correlations were found between the abundance of histological deposits and the Mascot confidence score ($\rho = 0.58$, $p = 0.10$), the PSM score ($\rho = 0.30$, $p = 0.43$) and the enrichment quantification ($\rho = -0.17$, $p = 0.66$).

Table 2 Identification and quantification proteomic results

Case No.	Amount of amyloid deposits	Proteins (Peptide spectrum matches, Mascot score, Ratio Amyloid/non-Amyloid)									Amyloid subtype by IHC	Amyloid subtype by PSM	Amyloid subtype by Mascot	Amyloid subtype (Ratio)
		Common protein			Precursors									
		APCS	APOE	APOA4	SAA	TTR	B2M	Lambda light chain	Kappa light chain	Other				
1	++++	3/152/**2.8**		3/131/**12.1**			3/113/**4.9**		**IGKC**2/77/**3.3**	**IGHG1**5/234/**0.8** **LYZ**5/239/**0.6** **IGHA2**1/37/**1.6**	Aβ2M	Equivocal	Equivocal	Aβ2M
2	++	4/150/**8.1**	2/76/**6.3**					**IGLC2** 2/102/**6.6**		**IGHG2**2/96/**4.5** **IGHA1**2/104/**2.2**	AL Lambda	Equivocal	Equivocal	AL Lambda
3	+++	9/498/**279**	14/592/**339**	10/469/**125**	**SAA2** 2/111/**19.6**					**IGHG1**4/181/**2.2** **IGHG3**4/175/**1.6** **IGHA1**3/144/**4.5**	AA	Equivocal	Equivocal (AH ?)	AA
4	+++++	5/242/**5.8**	26/1214/**185**	33/1410/**115**				**IGCL2**5/186/**0.6**	**IGKC** 4/344/**0.2**	**IGHM**15/562/**61.8** **FGA**6/383/**1.9** **IGHG3** 10/301/**2.6**	Non-informative	AH IgM	AH IgM	AH IgM
5	+++	45/663/**45.5**	30/1138/**118.2**	23/1051/**104.2**		26/735/**94.2**		**IGLV1-47**1/77/**2.4**	**IGKV3-20**3/174/**4.6**	**EFEMP1**4/259/**28.0** **APOA1**17/753/**0.9** **IGHG3**16/508/**2.5**	ATTR	ATTR	Equivocal	ATTR
6	+++++	23/675/**8.6**	68/1816/**13.6**	15/515/**2.0**		6/259/**3.4**		**IGLV3-9**1/129/**5.5**	**IGKV3-20**3/168/**2.1**	**APOC3**1/101/**7.7** **LYZ**8/257/**1.9** **FGA**26/813/**0.6**	AL Lambda	Equivocal	Equivocal	AL Lambda
7	+++++	12/614/**40.5**	41/1624/**50.8**	45/1713/**43.7**		12/549/**3.1**		**IGLV3-9**1/152/**0.9** **IGLC2**5/188/**0.44**	**IGKV6D-21**7/240/**15.5** **IGKC**35/768/**6.5**	**APOC3**2/164/**13.4** **APOA1**49/1431/**11.9**	Non-informative	AL Kappa*	AL Kappa*	AL Kappa
8	+++	10/336/**17.6**	4/38/**11.4**	11/281/**116.0**		3/97/**13.7**			**IGKV3D** 1/22/**2.9** **IGKC** 5/160/**1.9**	**IGHA2** NA/NA/**5.8** **LTF** 14/497/**3.4** **GSN** 10/344/**1.6**	Doubtful. ATTR?	AGel	AGel	ATTR
9	+++++	11/416/**369**	55/1330/**1363**	5/170/**169**		9/332/**72**			**IGKC** 8/414/**618**	**IGHM**9/296/**270** **GSN**10/348/**56**	AL Kappa	Equivocal	AL Kappa	AL Kappa

The amount of amyloid deposits was semi-quantitatively assessed in a + to +++++ scale where +++++ represents a sample with >80% of amyloid deposits. For each case, results from the common proteins found in amyloid deposits are firstly displayed, followed by the results of the top precursors of amyloidosis. For each protein, the number of peptide spectrum matches (PSM number of detected MS/MS spectra) is displayed, followed by the Mascot identification score and finally the enrichment in the amyloid area assessed by label-free enrichment quantification (abundance ratio between the amyloid microdissected area and the non-amyloid area, highlighted using bold fonts). Interpretations are provided for each approach, as well as the immunohistochemical findings. For each approach, the precursor with the best score was considered as the amyloid subtype (except for APOA1, commonly seen in amyloid deposits, asterisk). An equivocal result was considered when the second-best precursor score was in a 10% range from the first best precursor score (including ties). Abbreviations: Ig, immunoglobulin; IHC, immunohistochemistry; PSM, peptide spectrum matches; XIC, extracted ion chromato

Discussion

Accurate amyloidosis typing remains essential for guiding optimal therapeutic strategies. However, conventional histological methods, particularly immunohistochemistry on FFPE samples, are often limited by background staining, antibody unavailability, or tissue exhaustion when multiple stains are required. Consequently, laser microdissection of amyloid deposits followed by tandem mass spectrometry (MS/MS) has become the gold standard when conventional techniques fail. Two major MS-based workflows have been described for precursor protein selection, based on either Mascot identification scores or peptide spectrum match (PSM) counts. Yet, data interpretation can remain challenging, especially when multiple potential precursors are detected, partly due to the absence of true quantification. Although MS-based proteomics has revolutionized amyloid typing, only a few specialized centers have incorporated it into clinical practice. Even among these, difficult cases with several precursors of comparable identification confidence have been reported [11, 16, 26, 27]. In such studies, precursor selection relied primarily on either Mascot scores [11] or PSM numbers [16, 26, 28, 29] from a single microdissected region. While these methods are simple and require minimal postprocessing, their outputs reflect identification confidence rather than protein abundance, limiting interpretability in complex cases. In this work, we introduce XIC-based label-free enrichment quantification as an additional layer of information for amyloid precursor selection and demonstrate its potential value in challenging diagnostic contexts. Quantifying the enrichment of proteins between amyloid deposits and adjacent non-amyloid tissue provides a straightforward and robust way to discriminate the true precursor among multiple candidates. Moreover, unlike Mascot or PSM-based approaches, enrichment quantification could be more reliable in samples with limited deposits, as previous studies highlighting showed a decrease in PSM sensitivity when tissue availability is low [13, 30]. Whether this statement truly applies in the specific context of amyloidosis typing would require further studies. We observed lower overall PSM counts compared with published datasets, possibly due to differences in dynamic exclusion parameters, which were not always specified in previous reports. Our analyses were performed on microdissected amyloid and non-amyloid regions of equal surface area (1 mm^2 each), ensuring consistent material input and direct comparison between deposits and controls. This sampling strategy captures a deeper and more quantitative proteomic profile than the narrower sampling often used in reference workflows at the Mayo Clinic and UK National Amyloidosis Centre. By prioritizing quantitative over purely qualitative identification, our approach has the potential to increase the likelihood of accurate precursor assignment in difficult cases. Even when additional potential precursors are detected, enrichment ratios can distinguish the true amyloidogenic protein. In our series, enrichment quantification demonstrated superior robustness compared with Mascot or PSM-based methods. In all nine cases, the expected precursor was consistently identified as the most enriched protein within amyloid deposits, regardless of deposit size. In contrast, Mascot- and PSM-based approaches yielded less confident assignments in six cases. By applying a confidence score to precursor selection, we showed that enrichment quantification provided a higher level of diagnostic reliability, particularly in intermediate cases (e.g., cases 3–5), where traditional methods were ambiguous.

Interestingly, in addition to observing an enrichment of multiple precursor proteins within some deposits, several proteins not previously associated with amyloidosis were also enriched. Expanding proteomic profiling to larger patient cohorts could deepen our understanding of amyloid pathophysiology, as described in a recent study in the kidneys [31].

Our study has some limitations. Firstly, our study was limited to a small cohort of nine patients. Yet, it establishes a proof of concept for the diagnostic value of XIC-based label-free enrichment quantification. Further studies with larger cohorts will be needed to further confirm our findings. Secondly, the XIC-based method requires the availability of non-amyloid control tissue, with inherent additional required time and cost. Additionally, some amyloid samples do not contain an amyloidosis-free region. Although the quantification of an enrichment ratio can already allow for the comparison between an amyloidosis-rich and an amyloidosis-low region, using a normal sample (or a pool of samples) of the same tissue type from other patient(s) remains possible. Finally, the XIC-based method requires additional bioinformatics processing as compared to the Mascot and PSM-based methods. Still, this quantification approach is a well-established method in the field of proteomics.

In conclusion, our study provides a proof of concept that XIC-based label-free enrichment quantification can improve the accuracy and confidence of amyloidosis typing by MS-based proteomics. This method could offer a practical and quantitative enhancement to current workflows at the modest cost of analyzing an additional non-amyloid region and requiring basic bioinformatics integration. Enrichment quantification can thus be readily implemented as a first-line approach to minimize equivocal results, strengthen diagnostic confidence, and ultimately improve patient management.

Abbreviations

A	Amyloid
FDR	False Discovery Rate
FFPE	Formalin-fixed and paraffin-embedded
Ig	Immunoglobulin
IHC	Immunohistochemistry
LC-MS/MS	Liquid chromatography and tandem mass spectrometry
NA	Non-amyloid
PSM	Peptide spectrum matches
XIC	Extracted ion chromatogram

Supplementary Information

The online version contains supplementary material available at https://doi.org/10.1186/s12014-026-09598-0.

Supplementary Material 1

Supplementary Table 1

Acknowledgements

The authors wish to acknowledge the ARC Foundation for supporting the salary of Sylvaine Di Tommaso, and the Cancéropôle Grand Sud-Ouest (GSO) for the salary of Cyril Dourthe. We are also grateful to Marlène Maître (Laser Microdissection Platform, Magendie Institute, Bordeaux) and Nathalie Senant (Histology Platform, UAR TBMcore) for their valuable technical support.

Author contributions

SDT and BC participated in acquisition, analysis, interpretation of data and wrote the manuscript. SCT, BC and CD prepared figures , JWD participated in acquisition. CD and JW participated in the treatment and analysis of the data. FS, BLB and AAR designed the project, wrote the manuscript, drafted the work and revised it. All authors reviewed the manuscript.

Funding

Fondation ARC, Cancéropôle Grand Sud-Ouest (GSO), Région Nouvelle Aquitaine.

Data availability

The mass spectrometry proteomics data have been deposited to the ProteomeXchange Consortium via the PRIDE (22) partner repository with the dataset identifier PXD039814.

Declarations

Competing interests

The authors declare no competing interests.

Author details

[1]Univ.Bordeaux, Inserm UMR1312 BoRdeaux Institute of onCology (BRIC), Bordeaux F-33000, France
[2]Oncoprot Platform, TBM-Core US 005, Bordeaux F-33000, France
[3]Department of Pathology, Bordeaux University Hospital, Bordeaux F-33000, France
[4]Univ. Bordeaux, CNRS, ImmunoConcEpT, UMR 5164, Bordeaux F-33000, France
[5]Univ.Bordeaux, Proteomics Platform, Bordeaux F-33000, France

Received: 31 October 2025 / Accepted: 2 March 2026
Published online: 17 March 2026

References

1. Merlini G, Bellotti V. Molecular mechanisms of amyloidosis. N Engl J Med. 7 août. 2003;349(6):583–96.
2. Benson MD, Buxbaum JN, Eisenberg DS, Merlini G, Saraiva MJM, Sekijima Y, et al. Amyloid nomenclature 2020: update and recommendations by the International Society of Amyloidosis (ISA) nomenclature committee. Amyloid déc. 2020;27(4):217–22.
3. Benson MD, Buxbaum JN, Eisenberg DS, Merlini G, Saraiva MJM, Sekijima Y, et al. Amyloid nomenclature 2018: recommendations by the International Society of Amyloidosis (ISA) nomenclature committee. Amyloid déc. 2018;25(4):215–9.
4. Buxbaum JN, Eisenberg DS, Fändrich M, McPhail E, Merlini G et al. Amyloid nomenclature 2024: update, novel proteins, and recommendations by the International Society of Amyloidosis (ISA) Nomenclature Committee Amyloid. déc. 2024; 31(4):249 – 25.
5. Dasari S, Theis JD, Vrana JA, Rech KL, Dao LN, Howard MT, et al. Amyloid typing by mass spectrometry in clinical practice: a comprehensive review of 16,175 samples. Mayo Clin Proc. 2020;95(9):1852–64.
6. Wechalekar AD, Gillmore JD, Hawkins PN. Systemic amyloidosis. Lancet 25 juin. 2016;387(10038):2641–54.
7. Lavatelli F, Vrana J. Proteomic typing of amyloid deposits in systemic amyloidoses. Amyloid. 2011;18(4):177–82.
8. Satoskar A, Efebera Y, Hasan A, Brodsky S, Nadasdy G, Dogan A, Nadasdy T. Strong transthyretin immunostaining: potential pitfall in cardiac amyloid typing. Am J Surg Pathol. 2011;35(11):1685–90.
9. Hill MM, Dasari S, Mollee P, Merlini G, Costello CE, Hazenberg BPC et al. The Clinical Impact of Proteomics in Amyloid Typing. Mayo Clin Proc. mai. 2021;96(5):1122–7.
10. Colombat M, Holifanjaniaina S, Onifarasoaniaina S, Valleix S, Maisonneuve H, Kahn JE, et al. [Proteomics, a new tool for an accurate typing of amyloidosis]. Rev Med Interne mai. 2015;36(5):346–51.
11. Canetti D, Rendell NB, Gilbertson JA, Botcher N, Nocerino P, Blanco A et al. Diagnostic amyloid proteomics: experience of the UK National Amyloidosis Centre. Clin Chem Lab Med. 25 juin. 2020;58(6):948–57.
12. Rezk T, Gilbertson JA, Mangione PP, Rowczenio D, Rendell NB, Canetti D, et al. The complementary role of histology and proteomics for diagnosis and typing of systemic amyloidosis. J Pathol Clin Res juill. 2019;5(3):145–53.
13. Ankney JA, Muneer A, Chen X. Relative and Absolute Quantitation in Mass Spectrometry-Based Proteomics. Annu Rev Anal Chem (Palo Alto Calif). 12 juin. 2018;11(1):49–77.
14. Perkins DN, Pappin DJ, Creasy DM, Cottrell JS. Probability-based protein identification by searching sequence databases using mass spectrometry data. Electrophoresis déc. 1999;20(18):3551–67.
15. Mangione PP, Mazza G, Gilbertson JA, Rendell NB, Canetti D, Giorgetti S, et al. Increasing the accuracy of proteomic typing by decellularisation of amyloid tissue biopsies. J Proteom 8 août. 2017;165:113–8.
16. Mollee P, Boros S, Loo D, Ruelcke JE, Lakis VA, Cao KAL, et al. Implementation and evaluation of amyloidosis subtyping by laser-capture microdissection and tandem mass spectrometry. Clin Proteomics. 2016;13:30.
17. Matthiesen R, Carvalho AS. Methods and algorithms for quantitative proteomics by mass spectrometry. Methods Mol Biol. 2013;1007:183–217.
18. Ogawa M, Shintani-Domoto Y, Nagashima Y, Ode KL, Sato A, Shimizu Y, et al. Mass spectrometry-based absolute quantification of amyloid proteins in pathology tissue specimens: merits and limitations. PLoS One. 2020;15(7):e0235143.
19. Park J, Lee GY, Choi JO, Jeon ES, Kim K, Kim JS, et al. Development and Validation of Mass Spectrometry-Based Targeted Analysis for Amyloid Proteins. Proteom Clin Appl mai. 2018;12(3):e1700106.
20. Dourthe C, Julien C, Di Tommaso S, Dupuy JW, Dugot-Senant N, Brochard A et al. Proteomic profiling of hepatocellular adenomas paves the way to new diagnostic and prognostic approaches. Hepatology. 2021;74(3):1595-1610. https://doi.org/10.1002/hep.31826
21. Daubon T, Guyon J, Raymond AA, Dartigues B, Rudewicz J, Ezzoukhry Z, et al. The invasive proteome of glioblastoma revealed by laser-capture microdissection. Neurooncol Adv déc. 2019;1(1):vdz029.
22. Bouyssié D, Hesse AM, Mouton-Barbosa E, Rompais M, Macron C, Carapito C, et al. Proline: an efficient and user-friendly software suite for large-scale proteomics. Bioinf 1 mai. 2020;36(10):3148–55.
23. Henriet E, Abou Hammoud A, Dupuy JW, Dartigues B, Ezzoukry Z, Dugot-Senant N, et al. Argininosuccinate synthase 1 (ASS1): A marker of unclassified hepatocellular adenoma and high bleeding risk. Hepatology. 2017;66(6):2016–28.
24. Deutsch EW, Bandeira N, Sharma V, Perez-Riverol Y, Carver JJ, Kundu DJ, et al. The ProteomeXchange consortium in 2020: enabling « big data » approaches in proteomics. Nucleic Acids Res 8 janv. 2020;48(D1):D1145–52.

25. R Core Team. R: A Language and Environment for Statistical Computing [Internet]. R Foundation for Statistical Computing, Vienna, Austria. 2021. https://www.R-project.org
26. Vrana JA, Gamez JD, Madden BJ, Theis JD, Bergen HR, Dogan A. Classification of amyloidosis by laser microdissection and mass spectrometry-based proteomic analysis in clinical biopsy specimens. Blood 3 déc. 2009;114(24):4957–9.
27. Tasaki M, Ueda M, Obayashi K, Kinoshita Y, Matsumoto S, Mizukami M, et al. Identification of amyloid precursor protein from autopsy and biopsy specimens using LMD-LC-MS/MS: the experience at Kumamoto University. Amyloid mars. 2017;24(sup1):167–8.
28. Aoki M, Kang D, Katayama A, Kuwahara N, Nagasaka S, Endo Y, et al. Optimal conditions and the advantages of using laser microdissection and liquid chromatography tandem mass spectrometry for diagnosing renal amyloidosis. Clin Exp Nephrol août. 2018;22(4):871–80.
29. Holub D, Flodrova P, Pika T, Flodr P, Hajduch M, Dzubak P. Mass spectrometry amyloid typing is reproducible across multiple organ sites. Biomed Res Int. 2019;2019:3689091.
30. Bantscheff M, Lemeer S, Savitski MM, Kuster B. Quantitative mass spectrometry in proteomics: critical review update from 2007 to the present. Anal Bioanal Chem. 2012;404(4):939–65.
31. Charalampous C, Dasari S, McPhail E, Theis J, Vrana J, et al. A proteomic atlas of kidney amyloidosis provides insights into disease pathogenesis. Kidney Int. 2024;103(3):484–95.

Publisher's note